POLITECNICO DI TORINO
Repository ISTITUZIONALE

Thermal-hydraulic models for the cooling of HTS power-transmission cables: status and needs

(Article begins on next page)

20 April 2024

Thermal-hydraulic models for the cooling of HTS power-transmission cables: status and needs

Laura Savoldi[*], Daniele Placido and Sofia Viarengo

MAHTEP Group, Dipartimento Energia "Galileo Ferraris", Politecnico di Torino, Torino, Italy

[*] Corresponding author. E-mail: laura.savoldi@polito.it

Abstract

An overview of the main peculiarities of the models currently available in literature for the thermal-hydraulic analysis of the cooling of the HTS power transmission cables, mainly in nominal operating conditions, is performed. Several models address specific issues such as the temperature distribution along or across the cables, and their pressure drop, typically with a simplified approach. The verification and validation of the models has not been systematically addressed so far. From the analysis of the available literature, the lack of a general model, capable to address thermal-hydraulic transients for the cooling of the different possible cable designs, with capability to catch both the behaviour of the cable solid components and different cryogens, is highlighted. The main ingredients that such general thermal-hydraulic model should not miss are presented, also based on the know-how on, and comparison to, similar tools for LTS cables for nuclear fusion applications.

Keywords: HTS power cables, refrigeration, thermal-hydraulic modelling, numerical tools

Nomenclature

Symbol	Meaning	Unit
A	cross section	m^2
c	specific heat	$J\,kg^{-1}K^{-1}$
$\tilde{c}_v$	dimensionless specific heat at constant volume	~
f	friction factor	~
g	gravity acceleration	$m\,s^{-2}$
h	convective heat transfer coefficient	$W\,m^{-2}K^{-1}$
$\boldsymbol{H}$	magnetic field	$A\,m^{-1}$
I	current	A
k	thermal conductivity	$W\,m^{-1}K^{-1}$
$\dot{\tilde{m}}$	dimensionless mass flow rate	~
$\dot{m}$	mass flow rate	$kg\,s^{-1}$
$\mathcal{M}$	dimensionless mass	~
M	mass	kg
p	pressure	Pa
P	wetted perimeter	m
$\dot{q}$	linear heat transfer rate	$W\,m^{-1}$
$\mathcal{Q}$	dimensionless heat transfer rate	~
Q	heat transfer rate	W

Symbol	Meaning	Unit
$\dot{Q}$	volumetric heat transfer rate	$W\,m^{-3}$
r	radial spatial coordinate	m
t	dimensionless time	$\sim$
t	time	s
$\mathcal{T}$	dimensionless temperature	$\sim$
T	temperature	K
u	specific internal energy	$J\,kg^{-1}$
v	velocity	$m\,s^{-1}$
V	voltage	V
$\forall$	volume	m^3
w	specific enthalpy	$J\,kg^{-1}$
$\mathcal{W}$	dimensionless dissipated power	$\sim$
x	axial spatial coordinate	m

Greek letters

Symbol	Meaning	Unit
α	thermal diffusivity	$m^2\,s^{-1}$
ζ	zone length fraction	$\sim$
ρ	density	$kg\,m^{-3}$
τ	shear stress	$N\,m^{-2}$
ϑ	inclination of the cryostat	rad

Subscripts and superscripts

Symbol	Meaning
$|$	or
$\parallel$	along
$\perp$	across
c	critical
ch	channel
$cond$	heat transfer by conduction
$conv$	heat transfer by convection
Cu	copper
ext	external or environmental
f	liquid
frm	former
fg	two-phase
g	vapor
h	hydraulic
HTS	High Critical Temperature Superconductor
i, j	index for channels or solid components

in	Inlet, innermost or incoming
int	internal node
J	Joule heating
N_{VE}	last volume element
out	outlet, outermost or outgoing
p	constant pressure
PPLP	insulation layer
rad	heat transfer by radiation
rl	return line
sh	shield
sl	supply line
sol	solid component
tot	total
v	constant volume
wall	tube wall
η	generic segment, layer or node

1. Introduction

In the framework of the European Green Deal call for "supplying clean, affordable, and secure energy" (1), the path towards a clean energy transition is set with the boost of smart energy systems, providing high efficiency also in the generation and transportation of electricity, and a higher environmental sustainability (2). High critical temperature superconducting (HTS) Alternate Current (AC) and Direct Current (DC) transmission cables (SCTCs) and lines (SCTLs) could bring a clear size advantage and low total electrical losses for high-capacity transmission. They have the potential to address the need for more sustainable and efficient transmission, compared to solutions based on standard conductors (3).

The sustainability advantages of the HTS lines in terms of limiting the environmental (health and visual) impact and the destruction or alteration of the natural landscape, are clear (4). Despite the current capacities are still low, the SCTLs offer intrinsic advantages, for instance an easier and faster installation of the Superconducting (SC) cables, if compared to traditional resistive transmission ones. As pointed out in (3), the global design of SCTLs includes a pressurized coolant and refrigeration or compression stations along the line, as also the gas pipelines do. However, their typical transverse dimension of few tens of centimeters is smaller than that of gas pipelines, and the operating temperature is different (typically 15 K to 70 K, depending on the kind of HTS material considered). Despite the fact that several utilities around the world have already demonstrated their technical feasibility, no long SCTLs are currently in operation. High capacity connections in urban environments are so far the main application for HTS AC lines, while HTS DC, that lines could be used for high power

transmission over long distances, have been mainly adopted so far as a high-power link alternative to connect neighbouring asynchronous power systems (5).

The length of the proof-of concept superconducting lines, or of the lines already in operation, spans from few hundred meters up to 1-2 km. In South Korea, in the Shingal Project a 1 km-long, 23 kV AC HTS line has entered "commercial" operation in Yongin since late 2019 (6). That followed the successful demonstration of stability and operation condition of the two AC and DC cables in the real power grid in the Jeju island (7). In the city of Ishikari in the Hokkaido Island, Japan, two SC DC power transmission lines (one 500 m long and the second 1 km long, respectively) were successfully tested in 2015 and 2016 (8,9). In St. Petersburg in Russia a 2.5 km high-voltage DC SCTL is planned to enter operation into the city electric power system (2,10,11), and a full-scale transmission line has been recently tested, to confirm the design performance (12). In the German city of Essen, within the Ampacity Project a 1 km-long medium-voltage (10 kV) AC HTS line has been installed and successfully operated since 2014 as a connection of two electric substations, replacing a conventional high voltage system (13–15). In China, a 100 m-long 35 kV DC line was successfully tested in Tianjin (16), while a 1.2 km-long 35 kV AC SCTL is expected to enter into operation during 2021 (17). In the United States, the 600 m-long high-voltage AC SCTL is in operation since 2008 within the Long Island Power Authority Project (LIPA), originally aimed at demonstrating the commercial readiness of the system (18,19). HTS DC cables have a large retrofitting capability, and they have the potential to be used to integrate renewable energy sources with lines having a length of hundreds of kilometers. Unfortunately, projects like the Tres Amigas Project (20), betting on a long-length HTC DC high-power lines to "unite

the nation electric power grid" from the east to the west coast in the United States, are still looking for funding and have not become operational yet. The HTS DC SCTCs are also envisaged in applications to future all-electric ships (21,22) and aircraft (23), to meet the increasing electrical power demand at high power density.

Despite the fact that high-power HTS AC transmission or distribution systems have already proven their feasibility for dense urban areas and their present Technology Readiness Level (TRL) is estimated at 7 in (5), HTS AC cables have not widely entered the market yet. The same is *a fortiori* true for the HTS DC transmission systems, for which a TRL of 5 is estimated in (5) based on their limited testing within integrated systems. To reach the market maturity (TLR = 9) and penetration of the technology by the next few years, a substantial cost reduction has to be addressed, as well as the improvement of the system safety and reliability. For both aspects, the availability of reliable numerical models for the design, optimization and performance assessment in normal and off-normal conditions appears of paramount relevance (24). The development of numerical modeling in support of the HTS development, however, is still lagging somehow behind. Note that the proper cooling and, as a consequence, the thermal-hydraulic modelling, of the SCTCs and SCTLs is mandatory, since the capability to cool the SC material below the critical pooint with the lowest possible cryogen flow rate and pressure loss is enabling for the technology.

In the neighbouring field of nuclear fusion, the development of (low critical temperature, LTS) SC cables and magnets has been accompanied, in fact, over the past 25 years by the parallel evolution of numerical tools capable to capture the main features of such cables (25). Also for HTS SCTCs and SCTLs, the design and experimental tests should go along with the development and validation of numerical models, capable to capture the normal, as well as off-normal (fault currents, over-voltages,…) operating conditions. Such models should not only capture the steady state and transient electric behavior of the cables/lines, but they should also describe their (coupled) thermal-hydraulic behavior, as pointed out in (5). Once validated against experimental data, the numerical tools describing the thermal-hydraulic operation of the SCTCs and SCTLs could become an asset to flexibly design solutions with a high level of credibility.

The aim of this work is first to present a review of the numerical tools and models available for the thermal-hydraulic (cooling) analysis of AC and DC SCTCs, rewriting the models in terms of a common and unique nomenclature. For each model the level of approximation is described, highlighting if and how it has been validated against experimental data or anyhow benchmarked. The review leads naturally to identify the design needs that are still not covered by available models for a flexible and comprehensive thermal-hydraulic description of SC transmission cables and lines, which is the second aim of the paper.

The paper is organized as follows: different layouts are described for the HTS cables typically used for power transmission. Then, the review of the thermal-hydraulic models developed for them is introduced, moving from the most simplified models to the most complex. When the review is completed, the focus is shifted to the main features that a flexible thermal-hydraulic model should have, to help the SC power cable technology to move forward towards maturity.

2. Structure of HTS transmission cables

2.1 Layout

Given a target operating condition, the design of an HTS cable is the result of the trade-off between electrical efficiency, thermal and pressure losses in the cryostat and coolant line, and the use of superconductive material, with the aim of containing the system cost, guaranteeing at the same time a sufficient margin to off-normal operating conditions. From the topological point of view, all HTS transmission cables present a cable core made by one or more layers of HTS wires on a stabilizer *former*, then dielectric and insulation layers and a cryostat.

The structure of a typical HTS AC can first be classified according to the number of phases within the cryogenic envelope: a cable layout such as that of Figure 1a contains a single phase on a single-core, while the cable in Figure 1b contains three separate phases, each on its core. An AC SCTL with three separate cryogenic envelopes is suitable for high voltage conditions, while the presence of the three cores within a single cryostat (Figure 1b) is suited for low-medium voltage conditions, see also below. At low voltage, the three-phases, each made by several HTS layers, could also be concentrically wound around the "*former*" (either constituted by the coolant tube as in Figure 1a or by a copper cylinder, not shown). In the coaxial three-phases cable (see Figure 2) an electrical insulator is interposed among the HTS layers constituting the different
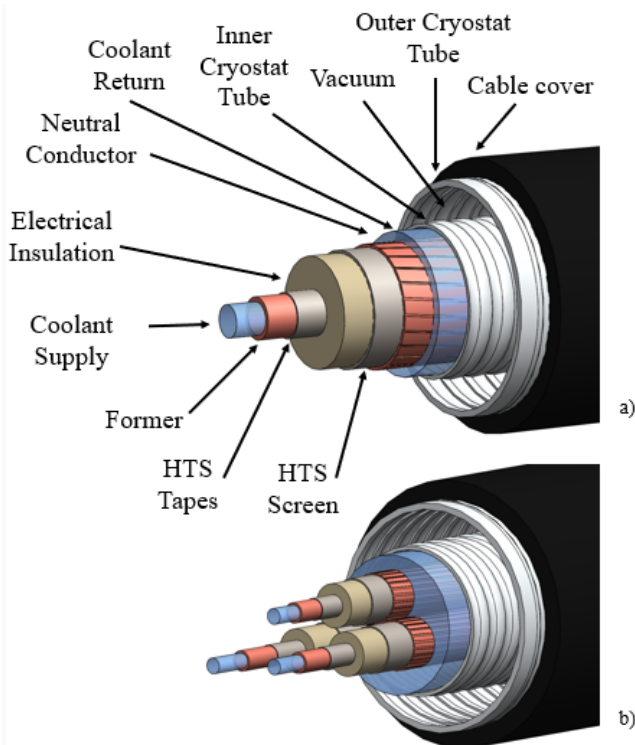

Figure 1. AC HTS cable design: single-core single-phase (a) and three -cores, each with one phases (b).
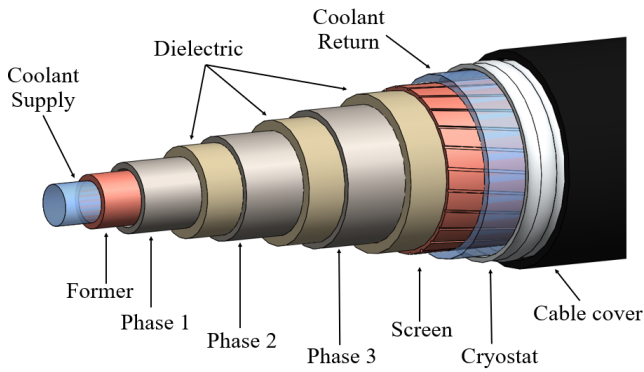
Figure 2. Three-phases coaxial HTS cable design.

phases. In all above-mentioned cases (single-phase, three-phases, either in coaxial configuration or on separate cores), a magnetic shielding is also present. The cryostat typically presents two concentric flexible (corrugated) tubes, separated by vacuum through a spacer. The buffer zone can be partially filled with layers of low emissivity insulation material, to increase the level of thermal insulation.

On the side of the HTS DC cables, there are still not defined standards for selecting their structure. In their basic configuration, however, various samples built and tested do not differ much from AC cables. Different configurations allow coping with the voltage level of the line: the two poles can be

Figure 3. Single-core HTS cable design: warm dielectric design cable (a) and cold dielectric design cable (b).

separated in two different cryogenic envelopes in the case of high voltage, or twisted inside the same envelope at medium voltages, or arranged in coaxial configuration at low voltages (26).

Another interesting feature that allows a classification of the HTS cables concerns the location of the dielectric, that can be either within the cryostat (cold dielectric, CD) or outside of the cryostat (warm dielectric, WD), as sketched in Figure 3 for a single-core case. The same concept can also be applied to a three-cores case, see Figure 4. In the WD architecture, the dielectric insulation, applied on the cryogenic envelope, is often made by cross-linked polyethylene (27) and remains at the ambient temperature. WD cables, with higher losses if compared to CD configurations, are suited for medium-voltage applications (28). In the CD configurations, typically PolyPropylene-Laminated Paper (PPLP) layers are adopted, at least for AC HTS cables. The insulation remains at the operating temperature of the HTS tapes/wires and the coolant laps it ("lapped insulation"). In view of the high voltage that could be reached by transmission lines, the dielectric strength of the cables needs attention. Note that in the lapped insulation the cryogen itself contributes to the dielectric strength of the cable.

As regards the superconducting material, the trend is moving from BSCCO toward second-generation (2G) HTS materials such as YBCO and MgB_2 (29): for YBCO, the reduction of HTS strand cost is still challenging, while, for MgB_2, the cryostat cost is crucial.

2.2 Cooling options

The cooling system of a SCTC includes a cooling station, the cable terminations and the cryostat with the coolant feeding lines. Note that, beside the coolant injection in the cable, terminations are components of particular interest, since they host the transition from HTS wire to copper leads and from cryogenic to room-temperature conditions. That implies that terminations typically cope with the shrinkage of the cable, and related stresses (26).

The coolant flows in the cable to provide the needed cooling against parasitic heat inflows and AC losses. A circulation pump or cold compressor, according to the type of cryogen, is installed in the circulating loop to ensure the desired flow rate and pressure. The cryogenic cooling system can operate either in an open loop or in a closed loop. In the
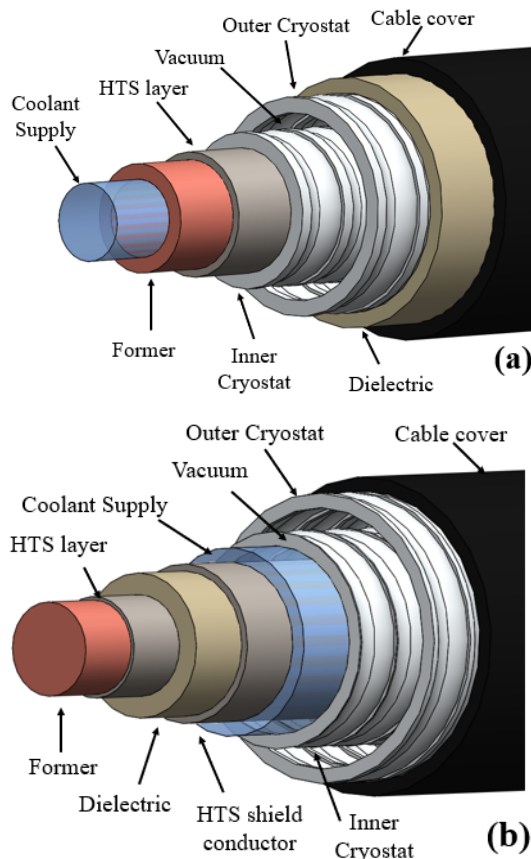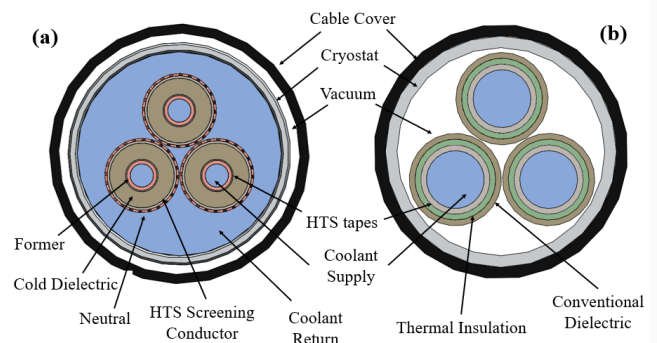

Figure 4. Multicore HTS cable design: warm dielectric (a) and cold dielectric (b) cable.
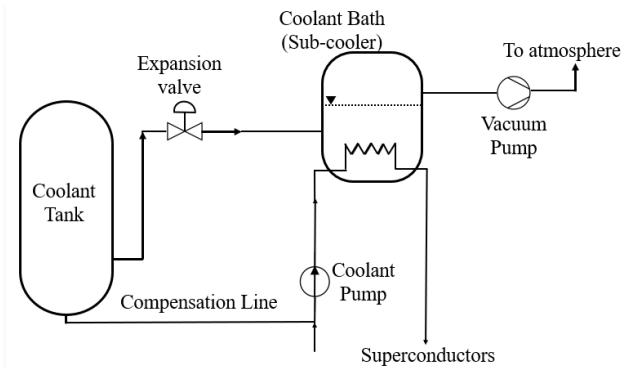
Figure 5. Open-loop cooling configuration for LN$_2$-cooled HTS cables.

first case, when the cryogen is liquid nitrogen (LN$_2$), a bulk LN$_2$ storage tank with a periodic refilling is used as the primary cooling source as reported in Figure 5, while in the latter cryocoolers are typically used. When the cable length is up to 2 km, the (cheaper) open loop configuration is preferred. When the cable length increases, the amount of LN$_2$ in the tanks becomes too large and a closed loop is typically adopted.

As far as the cooling configuration is concerned, the cryogenic system, including the cold circulator, can be located either at one or at both cable ends. If it is located just at one cable end, the coolant typically passes through the cable only once (supply side). An external feedback line brings then the coolant back to the cryoplant. In the case the length of the cable is sufficiently small, or a second cryogenic system is present at the other end of the cable, the return coolant can flow back inside the cable, either concentrically within the same core or within the other cores in case of a multi-core configuration with WD, see for instance Figure 2. In the case of CD, the use of cryogen can be twofold: from the one hand, it accomplishes the mission of keeping the HTS at the rated temperature in a dedicated channel. From the other hand the cryogen can contribute to enhance the dielectric strength. The two functions could be accomplished by two different cryogens as in some recent applications (29), see below.

Since 2G HTS materials have critical temperatures of ~90 K, the operating temperatures typically fall in the range of 50-70 K for transmission cables, to support the rated operating current in a compact design and/or to have a sufficient temperature margin in the case of unexpected heat loads and fault currents. Cooling is accomplished through cryogenic liquids such as liquid nitrogen (LN$_2$) in the temperature range of 65-77 K and pressure range of 0.3-1.5 MPa, which is the most commonly used coolant for SCTL operations due to its abundance, reduced cost, high electrical insulation, and large thermal capacity. However, in some cases the use of LN$_2$ is not suitable because of the need of a lower operating temperature, so that helium in gaseous phase (GHe) can be adopted. Furthermore, the use of GHe is typically envisaged in the SC cables in shipboard applications, where it is adopted and recommended to avoid the risk of asphyxiation in the event of a breach due to the confined space of such applications. Unfortunately, one of the drawbacks of using GHe as a coolant is its low dielectric strength, which can limit GHe-cooled SCTCs to low-medium voltage applications (30). A hybrid

configuration has been recently proposed within the European Project Best Paths (29), where the GHe acts only as the coolant, while the LN$_2$ is used as a part of the dielectric system.

3. Thermal-hydraulic models for HTS transmission cables

In this review, the models available in the published literature addressing the cooling of the SCTCs and SCTLs are reviewed, first translating them in terms of a common nomenclature, that allows for a thorougout comparison among them. The need for modeling one or two hydraulic channels for the coolant flow, or the arrangement of the layers across the cable depends on the specific cable layout under investigation, as shown in the previous sections.

The models are classified on the basis of the simplifications they perform on the spatial scales: both the transverse and longitudinal scales can present interesting features to analyze. For instance, the analysis of the temperature gradients across the cable section could reveal criticalities on the SC temperature, especially in faut conditions, while the analysis of the cryogen flow along the cable helps in evaluating the pressure drop and the global energy balance, mainly in normal operation. In the following sub-sections, different thermal-hydraulic models are presented, grouped in: one-dimensional (1D or 1D+) models, including pure radial and pure axial models or radial models for the solids coupled to axial model for the cryogen; two-dimensional (2D) models and three-dimensional (3D) models.

As far as the time scales are concerned, they span from the current faults one to that of the transit time within the cable. Accordingly, for each of the available models, the suitability to deal with fast transients such as current faults, rather than addressesing the operation of long cables in steady state, is commented.

3.1 Simplified 1D or 1D+ models

Very few zero-dimensional (0D) fully-lumped models have been adopted to describe the overall cable temperature evolution of HTS cable; among them, the model in (32) just solves a simple global heat balance for the coolant for a tri-phases co-axial cable in fault conditions, to compute the outlet and operating temperature.

Several 1D models along the cable length have been developed in the past 20 years. They take advantage of the spatial scale separation within the SC cables, where the longitudinal dimension is 3 to 5 orders of magnitude larger than the transverse one. That allows lumping the cable properties (HTS tapes temperature or coolant temperature for instance) across the whole cross section in a single variable.

A simple 1D **longitudinal** model only for the fluid (LN$_2$) of a cable with the supply and the return lines within the same cryostat is proposed in (33) for steady-state conditions. The supply and return lines for the incompressible coolant are both accounted for, and the heat transfer through the interposed insulation is considered. The SC temperature is not computed, but model also accounts for the electrical dissipation and parasitic heat entering the cable, see Eq. 1.

$$\dot{m}c_p \frac{dT_{sl|rl}}{dx} = \pm\dot{q}(x) + \frac{\dot{q}_J}{2} + \dot{q}_{ext} \qquad (1)$$

In Eq. (1) $\dot{m}$ is the mass flow rate, c_p is the specific heat at constant pressure (assumed constant), T is the temperature (subscripts sl and rl refer the supply and return lines, respectively), x is the axial spatial coordinate, $\dot{q}(x)$ is the heat rate per unit length transferred between the two streams (positive for the supply line and negative for the return line, respectively), $\dot{q}_J$ is the heat rate per unit length due to electrical dissipation and viscous friction, and $\dot{q}_{ext}$ the parasitic heat rate per unit length from the environment (only to the return line). The effect of the dielectric thermal conductance on the longitudinal temperature distribution are computed for a 2.5 km-length cable with a counter-flow cooling, and similarly it is done in (34) on a 1 km-long cable.

In (35), a 1D **longitudinal** thermo-fluid dynamic model is proposed to describe the steady-state behavior of different cryogens used as coolants in forced convection within SCTLs. The manipulation of 1D mass, momentum and energy conservation equations results in a couple of steady-state non-linear ordinary differential equations (ODE) in the independent variables density and temperature, as reported in Eqs. (2). Note that the coefficients are mainly derivatives of thermodynamic functions that can be easily computed from the analytical formulations of the thermophysical properties of the fluids. A variety of coolants can be used, since their thermophysical properties are calculated from analytical formulas as function of temperature and density, following the approach in (36). The solid components (HTS tapes, cryostat, insulation) are not considered directly, but their thermal effect on the cryogens is taken into account, allowing for the heating of the coolant mimicking Joule heating from the HTS tapes and parasitic heating from the environment.

$$v\left(\frac{\partial p}{\partial T} - \rho\frac{\partial w}{\partial T}\right)\frac{\partial T}{\partial x} + v\left(\frac{\partial p}{\partial \rho} - \rho\frac{\partial w}{\partial \rho}\right)\frac{\partial \rho}{\partial x} + \dot{Q}_J$$
$$+ \dot{Q}_{ext} = 0 \qquad (2a)$$

$$-v\frac{\partial p}{\partial T}\frac{\partial T}{\partial x} + v\left(v^2 - \frac{\partial p}{\partial \rho}\right)\frac{\partial \rho}{\partial x} - \dot{m}_s g\sin\vartheta$$
$$- v\frac{P}{A_{fl}}\tau = 0 \qquad (2b)$$

In Eqs. (2), $\dot{m}_s = \rho v$ is the specific mass flow rate (constant in time and space), ρ is the density, v is the velocity, p is the pressure, w is the specific enthalpy, $\dot{Q}_J$ and $\dot{Q}_{ext}$ are the internal volumetric heat generation and the external heat source per unit volume, respectively, g is the gravity acceleration, ϑ is the inclination of the cryostat with respect t the horizontal direction, P is the wetted perimeter, A_{fl} is the cross section in which the fluid flow through and, finally, τ is the shear stress, computed using correlations as, for instance, that in (37). The equations are solved by a fourth-order Runge-Kutta (RK) algorithm. That scheme, fully justified by the pure advective nature of Eqs. (2), does not however allow a trivial extension to include any equations describing the heat conduction in the solids, which is diffusive in nature, as well as to include any

time dependence. The model was used to address design analyses for the cooling of SCTCs.

A more complex model, also accounting for the solid components within the cable, is presented in (38). A **longitudinal** 1D transient for the enthalpy variation in the subcooled LN$_2$, as reported in Eq. (3a), is coupled in fact to a **longitudinal** 1D transient conduction model for the *former*/HTS tapes and HTS shield/stabilizing layer for any of the three phase in an AC cable (as that in Figure 1b) in Eq. (3b).

$$\frac{\partial w}{\partial t} + v\frac{\partial w}{\partial x} = \frac{1}{\forall\rho}Q \qquad (3a)$$

$$\rho_{(\eta)}c_{(\eta)}\frac{\partial T^{(\eta)}}{\partial t} = k_{(\eta)}\frac{\partial^2 T^{(\eta)}}{\partial x^2} + \dot{Q}_{in} - \dot{Q}_{out} \qquad (3b)$$

Eq. (3a) refers to the coolant: t the time, $\forall$ is the coolant volume and Q the heat rate. Eq. (3b) refers to the $(\eta - th)$ solid component under consideration (copper *former* or HTS tapes): k is the thermal conductivity, c the specific heat, $\dot{Q}_{in}$ and $\dot{Q}_{out}$ are the heat rate per unit volume entering and exiting the component, respectively. The coefficients for the solid-components in Eq. (3b) are assumed constant. The pressure in the coolant along the cable is also modelled as in Eq. (4). That allows evaluating the coolant temperature, knowing its pressure and enthalpy, through the commercial package GASPAK (39).

$$\frac{dp}{dx} = -2f\frac{\rho v^2}{d_h} \qquad (4)$$

In Eq. (4), f is the Fanning friction factor (a dimensionless parameter for the evaluation of the distributed pressure drop in a conduit) and d_h the hydraulic diameter. The model was applied to analyse the transient temperature distributions in HTS cables after a fault. The computed temperature evolution was compared to experimental data finding a reasonable agreement at certain locations along the investigated cable.

A similar 1D **longitudinal** model for the solid components is presented in (40) to analyze fault conditions in the "Asahi cable" (41), with a similar lay-out as in Figure 1b. Again, 1D time-dependent heat conduction equations as Eq. (3b) are considered in the longitudinal direction separately for the *former* / HTS tapes and for the shield elements.

$$\dot{Q}_{in,HTS} = \dot{Q}_{J,HTS} \qquad (5a)$$

$$\dot{Q}_{out,HTS} = \dot{Q}^{cond}_{HTS\rightarrow PPLP} - \dot{Q}^{conv} \qquad (5b)$$

The volumetric source/sink terms are given in Eqs (5) for the HTS layer. $\dot{Q}_{J,HTS}$ keeps into account the Joule heating by fault currents in the conductor, $\dot{Q}^{cond}_{HTS\rightarrow PPLP}$ is the heat transferred by conduction between the HTS layer and the insulation, $\dot{Q}^{conv}$ is the heat transferred by convection between the HTS layer and the fluid. (Similar source/sink terms, *mutatis mutandis*, are written for the shield element). The heat released to the coolant is modeled by suitable convective heat transfer coefficients, obtained through the well-known Dittus-Boelter correlation. For the coolant, a local enthalpy balance is computed at each time step. The global pressure increase in time is evaluated by a simple 0D model, which accounts for the evaporation of LN$_2$ due to faults. A very similar model, with

equations for more solid components and a slightly different cable layout is proposed in (42), and solved by Finite Differences Method (FDM). It is applied not only to assess the effects of short-circuit accidents on a three-cores AC cable, but also to the analysis of normal operating conditions.

In (43) a CD cable, constituted by one inner and one annular LN$_2$ channels with a copper *former*, the HTS and the shield/insulation, is considered. Along the conductor, a simple 1D steady-state enthalpy balance is considered for both fluid channels. Since, however, in the terminations parasitic heat and Joule heat enter the cable through the copper current leads, the modeling of the terminations is considered of paramount importance and it is added to the cable model.

A completely different simplification of the spatial scales involved in the analysis of the SCTCs and SCTLs is done in several other models that discard the spatial distribution along the cables to concentrate on the radial temperature distribution across the cable section.

A 1D transient conduction model for a CD cable with a copper *former* (see Figure 4.b) is written in (44), considering only the **radial** direction and a constant thermal conductivity, see Eq. (6), where r is the radial spatial coordinate and α is the thermal diffusivity (constant in each layer of the cable).

$$\frac{1}{\alpha}\frac{\partial T}{\partial t} = \frac{\partial^2 T}{\partial r^2} + \frac{1}{r}\frac{\partial T}{\partial r} + \frac{\dot{Q}}{k} \qquad (6)$$

At the interface with the coolant, a convective boundary condition is imposed. The volumetric source term $\dot{Q}$ is computed by an electro-magnetic coupled analysis, highlighting the importance of such multi-physics analysis, well-known in the field of SC cables for nuclear fusion applications (45). The model is applied to the assessment of the temperature profile across the cable in case of normal and off-normal (fault current) operating conditions. A 1D transient model for the temperature in the radial direction for a similar cable is also presented in (46), aiming at evaluating the temperature distributions in the HTS cable layers under normal operating conditions.

A 1D steady-state **radial** conduction model for each layer of the coaxial AC cable in Figure 2 is proposed in (47), for the analysis of the operating regime, see Eq. (7), where the superscript (η) is referred to a generic layer.

$$\frac{d^2 T^{(\eta)}}{dr^2} + \frac{1}{r}\frac{dT^{(\eta)}}{dr} + \frac{\dot{Q}^{(\eta)}}{k^{(\eta)}} = 0 \qquad (7)$$

Note that the source term due to AC losses is included here, while the conductivity k is assumed constant in each layer (η). The solution of the differential problem is achieved by means of the FDM. The model is used to check the safe operation of the cable, with the LN$_2$ temperature in the inner cryostat not exceeding 78 K, in normal operation and fault current conditions. A similar model, proposed in (48), allows considering different HTS layout, with or without a separate retun line for the LN$_2$ coolant, modeling a steady-state enthalpy balance for the fluid in the longitudinal direction. The pressure losses along the supply and return lines are computed using the Darcy-Weisbach constitutive relation for the pressure drop, by suitable definition of the friction coefficients.

Putting together the need to control the temperature gradient across the cable and the temperature evolution of the coolant along the cable, the authors of (49) propose, for the analysis of the coaxial AC cable design of the Ampacity project (13), a 1D + 1D model. A steady-state 1D radial heat transfer conduction model (with constant thermal conductivity) for each layer (i.e., inner tube, 3 layers of HTS with interposed PPLP, and the copper screen) is coupled to a 1D axial transport model for an incompressible coolant, as reported in Eq. (8).

$$\frac{dT_{sl|rl}}{dx} = \pm \frac{h_{sl|rl}\pi d_{sl|rl}\left(T_{sl|rl}^{wall,\parallel} - T_{sl,rl}\right)}{\dot{m}c_p} - \frac{\dot{q}_{ext}}{\dot{m}c_p} \qquad (8)$$

In Eq. 8, h is the convective heat transfer coefficient, d is the effective diameter of the channel and $T^{wall,\parallel}$ is the wall temperature along the cable. The minus sign at the Right Hand Side (RHS) holds for the return line rl in the corrugated annulus. The first term at the RHS accounts for the heat transfer at the inner side of the annular channel, and the latter for the specific external heat load $\dot{q}_{ext}$ per meter along the cable length on the outer side of the annular channel. Note that for the rl the flow is in the negative x direction. The conduction models are matched at the interface between the different layers imposing continuity of the temperature (no contact thermal resistances) and of the heat flux. In this way the 3D thermal-hydraulic problem of the cable is simplified in a **1D (radial) + 1D (axial)** problems. The resulting model is able to evaluate the steady-state temperature distribution along and across the cable, accounting for heat transfer by conduction and convection across the cable, considering at the same time the advection along the cooling channels. Note that the source terms in Eq. (8) do not explicitly account for, e.g., AC losses, but they could be easily included in the external load. As far as the hydraulic model is concerned, the pressure losses occurring both in the inner tube (supply line) and in the annular duct (return line, see Figure 1a) are again calculated using the Darcy-Weisbach constitutive relation. The model has been used to simulate the operating range of the Ampacity cable as a function of mass flow rate, inlet temperature and outlet temperature of the coolant. In both (47) and (49), the authors show that the temperature is uniform in the SC layers, while temperature gradients are faced in the insulation layers, in view of their reduced thermal conductivity, as expected.

Another interesting **1D + 1D** model is presented in (50), where a radial *transient* model for the solid components is coupled to an axial 1D model for the fluid flow, which includes a transient mass/momentum and energy conservations laws for a compressible fluid. The model is utilized to evaluate the recovery time after a fault and quench of a co-axial three-phase cable. The evolution of the temperature gradient along the cable is computed until the steady-state operation is recovered.

A detailed investigation of the pressure drop along different configurations of the cooling systems of a tri-axial cable (with both internal and external return lines) is reported in (51), where major losses are obtained by an ad-hoc Computational Fluid Dynamic (CFD) modelling and minor losses account for cable bending and snake path. A network model for the configuration with an internal return line is developed. Diffusion nodes, related to solid components (HTS layers, stabilizer, insulation), are connected each other and to junction nodes, which account for the fluid. The expanded 1D network is then solved using the commercial software SINDA/FLUINT (52). The model is used for design purposes to compute and

compare the thermo-dynamic trajectories of the fluid pressure and temperature along the cable for the different configurations.

Although remaining in the 1D category, the thermal-hydraulic model presented in (53) is very interesting. In fact the model, developed in the MATLAB Simscape environment, solves the energy conservation law for the different solid components (HTS, insulator and steel layers), as well as transient mass and energy conservation laws for the LN_2 coolant, see Eqs (9).

$$\forall \frac{d\rho}{dt} = \dot{m}_{in} - \dot{m}_{out} \qquad (9a)$$

$$M \frac{du_{out}}{dt} = \dot{m}(w_{in} + w_{out}) + Q \qquad (9b)$$

In Eq. (9b), u is the specific internal energy, M is the mass while Q is the total heat rate transferred between the fluid and the tube wall. The subscripts in and out refer to the inlet and outlet, respectively. Exploiting the available 3-Zone Pipe block model, the cable is discretized in segment, and Eqs. (9) are written for each pipe segment (i). The time derivative in Eq. (9a), accounts also for possible two-phase flow and compressibility effects as shown in Eq. (10) for the generic cable segment i:

$$\frac{\partial \rho^{(i)}}{\partial t} = \left(\frac{\partial \rho^{(i)}}{\partial p}\right)_u \frac{\partial p^{(i)}}{\partial t} + \left(\frac{\partial \rho^{(i)}}{\partial u}\right)_p \frac{\partial u^{(i)}}{\partial t} + \rho_f^{(i)} \frac{d\zeta_f^{(i)}}{dt}$$
$$+ \rho_{fg}^{(i)} \frac{d\zeta_{fg}^{(i)}}{dt} + \rho_g^{(i)} \frac{d\zeta_g^{(i)}}{dt} \qquad (10)$$

In Eq. (10), ζ is a zone-length fraction (i.e., the space occupied by a specific phase), while f, fg and g represent the liquid, the two-phase and the vapour states, respectively. The flow is assumed to be fully developed. A boundary-following model predefined in Simscape allows tracking the aggregation state (liquid or vapour) of the coolant within the cooling channels. The source term for the energy equation, Eq. (9b), is capable to capture the heat transfer in single or two-phase flow by mean of suitable correlations. A simplified steady-state momentum conservation law is also written for the entire conductor length. The model in (53), benchmarked against a CFD simulation, is coupled to an electric model which accounts for the SC properties of the HTS tapes, and it is applied to a case study where a sudden cryostat vacuum loss induces cryogen boiling and two-phase flow. The global coupled model appears very flexible, with the only clear weak points of being tested only for nitrogen coolant and of relying on a commercial software.

3.2 2D models

A simplified physical model for the analysis of the cooling of the SCTCs, which combines principles of classical thermodynamics and heat transfer, is developed starting from the 3D (or 2D axy-symmetric) differential equations describing the transient thermal-hydraulic behavior of the cable. The cable cross section is discretized in elements as reported in Figure 6 for an axy-symmetric configuration, and the equations are discretized in space using a 3D (or 2D) cell-centred Finite
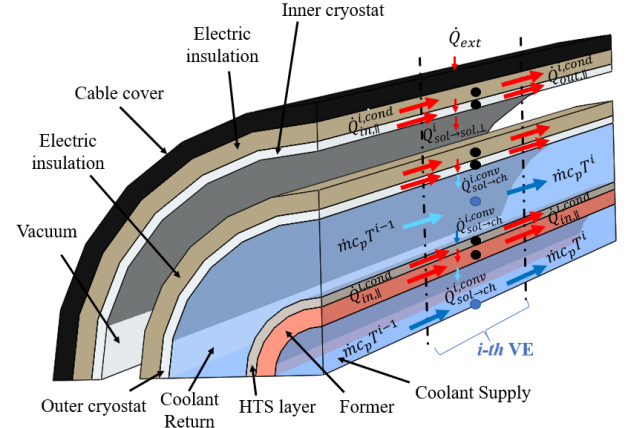

Figure 6. Schematic representation of the VEM discretization of an HTS cable. The solid circles identify the VE centre, the arrows show the contribution to the heat transfer.

Volume (FV) scheme. The heat fluxes coming from the neighbouring cells are integrated for each volume, resulting in the so-called Volume Element Model (VEM), quite popular for the HTS cables for power transmission.

A VEM was first proposed by Souza et al. in (54) for HTS DC cables for naval applications (which are gas cooled, see above), both for steady-state and transient conditions. The reference configuration of the cable is reported in Figure 6. It can be noted that all the layers are concentric, neglecting the channels spacers by the assumption that they are small enough not to affect the thermal behavior of the cable. Separate Volume Elements (VEs) are attributed to each layer (except to the vacuum layer, which is ignored). After the integration of the energy conservation law in each VE, a set of coupled ODE in the form of Eqs (12)-(13) is found, applying an explicit numerical scheme.

$$M^{(\eta)} c_v^{(\eta)} \frac{\partial T^{(\eta),i}}{\partial t} = \sum_{sol} Q_{sol \to ch}^{i,conv}$$
$$+ \dot{m}^{(\eta)} c_p^{(\eta)} \left(T^{(\eta),i} - T^{(\eta),i-1}\right) \qquad (12)$$

$$M^{(\eta)} c^{(\eta)} \frac{\partial T^{(\eta),i}}{\partial t} = Q_J^{(\eta)} - \sum_{ch} Q_{sol \to ch}^{i,conv} + \sum_{sol} Q_{sol \to sol,\perp}^i$$
$$+ Q_{in,\parallel}^{(\eta),i,cond} - Q_{out,\parallel}^{(\eta),i,cond} \qquad (13)$$

Eq. (12) and Eq. (13) are written for the (η) fluid channel and solid layer/component, respectively. The index i refers to the i-th VE in the longitudinal (axial) direction. The coefficient c_v is the specific heat at constant volume. The subscripts in and out are related to the incoming and outgoing fluxes of the i-th VE, respectively, while J refers to the heat generation rate in the SC. The coupling terms at the RHS of Eqs. (12)-(13) hide the conduction, convection and radiation thermal exchanges, which are suitably considered, see Figure 6, taking into account different operational, environmental and design conditions by theoretical and empirical correlations. More in detail, for the coolant in Eq. (12), the advection along the channel is accounted for in the last term, while the term $Q_{sol \to ch}^{conv}$ accounts for the heat rate transfer by convection between the fluid

(subscript *ch*) and the solid elements coupled to it (subscript *sol*) through suitable correlations for the heat transfer coefficients. In the equation for the solid elements (Eq. (13)) the term $Q_{\parallel}^{cond}$ accounts for the thermal conduction *along* the cable, while the term $Q_{ch \to sol}^{conv}$ accounts for the heat transfer by convection, and finally the term $Q_{\perp}$ accounts for the heat transfer by conduction and/or radiation *across* the cable. This is the first model where the parasitic heat from the environment is computed directly modelling the radiative contribution according to the Stefan-Boltzmann formulation, and not just assuming a constant value of the heat flux entering the cable.

The properties of the coolant (GHe in (54)) are function of temperature and pressure. The specific heat and thermal conductivity of the solid components are also considered as functions of the temperature. For the resulting set of ODE, the Newton-Raphson and RK methods are used for the steady-state and transient numerical solution, respectively. The capability to also capture accurately the temperature gradients around a hot spot is enabled by the use of a static non-uniform spatial grid along the axis. In (55) the same model is applied to investigate the cool-down time of the cable, with various GHe flow rates. The work in (54) is extended also in (56) and (57) to include a 1D equation for the pressure drop along the GHe cooling channels, the differential form of which is reported in Eq. (14).

$$\frac{dp}{dx} = f \frac{\rho v^2}{2 d_h} \qquad (14)$$

The coolant density ρ in Eq. (14) is computed as a function of the local temperature and pressure, while the coolant velocity v is obtained from the mass flow rate given in input. The friction factor f is selected from correlations to properly account for the different kinds of channels present on the HTS cable (central tube, annular channel, …). With the capability of computing the pressure drop, the evaluation of the pumping power has been introduced in this model, which can be used for the design of the cables.

The dimensionless formulation of the VEM, first presented in (58), has been further developed in (24). Eqs. (12) and (13) have been re-written in dimensionless form, as shown in Eqs. (15) and (16), respectively:

$$\mathcal{M}^{(\eta),i} \tilde{c}_v^{(\eta),i} \frac{\partial \mathcal{T}^{(\eta),i}}{\partial t} = \left[\sum_{sol} \mathcal{Q}_{sol \to ch}^{i,conv} + \dot{m}^{(\eta)} \left(\mathcal{T}^{(\eta),i} - \right) \right. \\ \left. - \mathcal{W}^{(\eta)} \right] \qquad (15)$$

$$\mathcal{M}^{(\eta),i} \tilde{c}^{(\eta)} \frac{\partial \mathcal{T}^{(\eta),i}}{\partial t} = \left[\mathcal{Q}_J^{(\eta)} - \sum_{sol} \mathcal{Q}_{sol \to ch}^{i,conv} + \sum_{sol} \mathcal{Q}_{sol \to sol,\perp}^{i} \right. \\ \left. + \mathcal{Q}_{in,\parallel}^{(\eta),i,cond} - \mathcal{Q}_{out,\parallel}^{(\eta),i,cond} \right] \qquad (16)$$

where $\mathcal{T}$ represent the dimensionless temperature, t is the dimensionless time, $\mathcal{Q}$ is the dimensionless heat transfer rate, $\dot{m}$ is a dimensionless mass flow rate ($\dot{m}^{(\eta)} = \dot{m} c_p / hA$), $\mathcal{M}$ and $\tilde{c}_v$ are derived from the mass and the specific heat at constant volume, respectively, both made dimensionless by proper scaling to reference quantities. In Eq. (15) for the

coolant, the power to overcome friction is hidden in the term $\mathcal{W}$, which represents the dimensionless power dissipated by friction.

The model was calibrated (emissivity of the insulation layer, for instance) and validated against experimental results coming from the test of a 30 m-long YBCO cable at Florida State University (59). The mathematical formulation, for dimensionless temperatures, is translated into a constrained optimization problem, where the constraint is set on the cryostat cross section, which is kept constant. The objective function is the minimization of the sum of the cryogenic cooling power $\mathcal{Q}_{cryo}$ and pumping power $\mathcal{W}_{tot}$, computed in dimensionless form in Eqs. (17) and (18), respectively.

$$\mathcal{Q}_{cryo} = \sum_{(\eta)=1}^{ch} \dot{m}^{(\eta)} \left[\mathcal{T}^{(\eta),N_{VE}} - \mathcal{T}^{(\eta),1} \right] \qquad (17)$$

$$\mathcal{W}_{tot} = \sum_{(\eta)=1}^{ch} \sum_{i=1}^{N_{VE}} \mathcal{W}^{(\eta),i} \qquad (18)$$

With this model, the authors of (24) were able to compute the optimal operating and design parameters, and namely the GHe flow rate and the ratio between the annular space for GHe flow and the vacuum space. A different model of the same HTS cable, and namely a 2D model of the turbulent flow via Computational Fluid Dynamics, CFD, is presented in (60) by the same authors of (59) but limited to the cable terminations, aiming at better understanding the thermal aspects related to the complex structure of those regions.

In (61), the layout of a cable cooled by LN₂ is addressed using the VEM model to predict both its steady-state and transient behavior. The model was applied to a cable of the Electric Power Research Institute (EPRI) (62). The power generation within the cable is considered there by properly accounting for the current-voltage characteristic of the HTS tapes. When a loss of superconductivity takes place, heat is generated in any conductive layer within the cable. The model was applied to the investigation of the effects of varying flow rates and coolant flow directions, including the possibility of having counterflow of the coolant in the two channels, achieving the evaluation of the maximum cable length for reliable operation.

The VEM is shown to be easy to combine with a Finite Difference Time-domain (FDTD) electric analysis in (63) for the analysis of transient conditions such as short-circuits, cable energizations and lightning surges. At each time step the FDTD model computes the current in each cable segment, which is used to compute the Joule losses on the conducting layers, considering the temperature-dependent resistivity of the different layers and an approximation of the SC characteristic.

The radial discretization adopted in the VEM (57) for the HTS DC cable cooled by GHe is also adopted by (64) to identify different regions in a 2D Finite Element Method (FEM) model implemented in COMSOL Multiphysics. The GHe turbulent flow is modelled with CFD using a simple κ-ε turbulence closure. The model, validated against steady-state experimental data (59), has been used to perform transient analysis for different off-normal operating conditions (vacuum break, cryocooler failure, cryocooler and gas circulation

impeller failure), allowing the test of possible mitigating strategies.

The model presented in (65) and further developed in (66) relies on a 2D axysimmetric transient conduction equations for the solid components of a three-phases coaxial HTS cable (as in 2). The corresponding Partial Differential Equation (PDE), reported in Eq. (19), is written assuming all material properties as constant, and it is coupled to the transient advection equation for the uncompressible fluid (LN$_2$) in the supply and return line. The fluid is assumed inviscid, see Eq. 20.

$$\frac{1}{\alpha}\frac{\partial T}{\partial t} = \frac{\partial^2 T}{\partial r^2} + \frac{1}{r}\frac{\partial T}{\partial r} + \frac{\partial T^2}{\partial x^2} + \frac{1}{k}\dot{Q} \qquad (19)$$

$$\rho c\,\frac{\partial T_{sl|rl}}{\partial t} \pm \rho c v_{sl|rl}\,\frac{\partial T_{sl|rl}}{\partial x}$$
$$= \frac{h_{sl|rl}P_{sl|rl}\left(T_{frm|Cu} - T_{sl|rl}\right)}{A_{frm|Cu}} \qquad (20)$$
$$+ \frac{\dot{q}_{ext}^{rad}}{A_{frm|Cu}}$$

In Eq. (20) P the cryostat perimeter, A the cross section and $\dot{q}_{ext}^{rad}$ is the external radiation rate per unit of length (considered just for the return line). The subscripts $sl|rl$ denote the supply or return line, respectively, while $frm|Cu$ stands for the *former* or *copper*, when the supply or return line are considered, respectively. At the Left-Hand Side (LHS) of the equation, the positive sign is used for supply line, while the negative sign is adopted for the return line. The set of equations is solved using the FDM and it has been applied to investigate the temperature increase of the cable after a fault transient. The model was able to show that the heat propagation inside the cable takes place on a time scale much longer than that of the fault itself, driven by the diffusion time in the different material layers, coupled to the advection time throughout the supply and return line. In (66), the model is further developed by introducing an Alternative Direction Implicit (ADI) technique for the numerical solution of the FD problem. The evaluation of the pressure drop along the entire cable is also added, motivating the adequacy of a global (as opposed to local) evaluation for the pressure drop by the reduced variation of the coolant density in the operational space for the LN$_2$. A remarkable peculiarity of the model in (66) is that it is offered to the scientific community as an open-source tool.

A 2D FEM model, coupling the fluid and the solid regions through an energy balance, has been applied in (67) for different three-phases SCTCs in normal operation in steady-state condition, showing again that the radial discretization for the temperature could be useful only for the insulation region.

3.3 3D models

In (68) a time-dependent 3D FEM pure thermal analysis of an AC three-phase HTS SCTC is reported, where the coolant is accounted for only as a boundary condition for the copper shield layer of the cable. The analysis is performed on a very short length of the cable because of its computational cost, since the entire cable cross section is considered in the simulations. The evaluation of the dynamic thermal stability of the cable aimed at identifying the intervention conditions of the protection system in case of off-normal operation such as,

for instance, fault currents. Note that, even if the model is 3D, it refers to an axysimmetric configuration, for which a 2D analysis would have returned the same results: the need for a 3D model is not justified.

Recognizing the relevance of heat transfer and fluid flow dynamics of the coolant (LN$_2$) flowing in a DC CD cable configuration, the authors in (69) address the LN$_2$ flow pattern for a case when the cable core is eccentric within its cryostat-tube. The use of a 3D model is justified in this case by the lack of any symmetry. The commercial FV software FLUENT was used to evaluate the effect of the eccentricity of the cable core on the pressure drop and the temperature distribution in a DC high-voltage cable. Some non-negligible differences with respect to the pressure drop computed for the same cable if it was concentric were found.

4. Discussion

The review above shows how many different models, from very simple to very complex, have been developed for the analysis of thermal-hydraulic transients for HTS cables for power transmission, though with different scopes. A summary of the models along the timeline is reported in Figure 7, showing that, rather than progressively switching from 1D to 2D models, a blending of different models coexists in the last decade. The most used models include some (at least) macro-discretization of the cable cross section, to capture transverse gradients (mainly identified in the insulation layers). Moreover, the capability to capture variations of HTS and cryogen temperature along the cables by longitudinal energy transport equations is included in most models. As far as the thermophysical properties of the coolants are concerned, typically the LN$_2$ flow is assumed single-phase and uncompressible. The latter assumption, which could be reasonable for the LN$_2$ case, is typically adopted also in the case of GHe, for which compressibility effects may, however, play a role. As far as the thermophysical properties of the solid components are concerned, constant properties of the *former* and insulation are usually considered, in view of the small temperature variation allowed or expected in normal operating condition. For the HTS layers, a simplified recipe in the evaluation of the power possibly dissipated by Joule effect is adopted in few models. Most models neglect in fact the relation
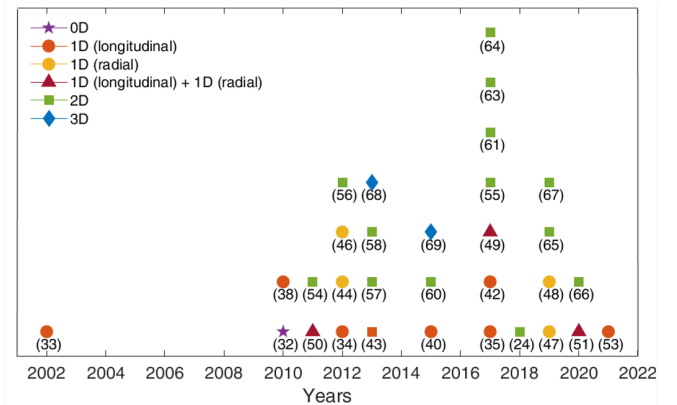

Figure 7. Schematic representation of the timeline of the development of the thermal-hydraulic model reviewed in the paper, with the detail on the type (dimensionality) of the models.

between the magnetic field (**H**), critical current (I_c) and temperature (*T*). The parasitic load from the environment is typically included in the form of a given constant value. From the numerical point of view, as far as the spatial discretization is concerned, only static spatial grids (but not necessarily uniform) have been adopted in the models analysed here.

With the additional know-how that comes from the experience gained in the modelling of LTS cables for fusion applications, see (25,45,70,71) and reference therein, the features that could ensure robustness and flexibility to a comprehensive model for the HTS SCTCs are summarized below.

- Capability to solve the transient energy conservation law for each different solid component along and across the cable axis, lumping each component in a separate thermal element. The thermal coupling between the different thermal elements should be flexible to account for different cable topologies and should account for conductive and/or radiative mechanisms. While pure 1D radial models are not suitable for that, 1D longitudinal models accounting for different components in a lumped way, as well as 1D+1D and 2D models, could successful implement this feature.

- Capability to solve the transient mass, momentum and energy conservation laws along the cable axis for each different coolant channel (1D), assuming a uniform thermal-fluid-dynamic state across the channel cross section. In fact, the hydraulic behaviour of the cable in the large majority of the cases of interest can be satisfactory modelled with reference to the average velocity on the channel cross section. Similarly, the heat removal and transfer can accurately rely on the average coolant velocity and on its average temperature on each cross section. The thermal coupling to the different thermal elements describing the solid components (bullet above) should account for convective mechanisms through suitable heat transfer coefficients / correlations, possibly cross-checked by dedicated experimental or numerical tests, as done for LTS cables for fusion. 1D longitudinal models accounting for the thermal coupling to the neighbouring solid components can be suited for the analysis of the transient behaviour of the coolant channels, when a 2D modelling of the cable is not pursued.

- Capability to consider the peculiarities of different plausible cryogens. Since the two major players are LN_2 and GHe, the conservation laws should be formulated to account for some simplified model for the transition from liquid to vapour phase in the case of LN_2 and to include compressibility effects in the case of GHe. These features should enable a more accurate evaluation of the pressure drop along the cable.

- Capability to simulate different operating conditions, in a wide temperature range. That implies the need for including the temperature dependence of the material properties, as typically done for the LTS cables to cope with the non-linearities of the properties in the temperature range of normal and off-normal operation (quench conditions).

- Inclusion of a sound description of the AC losses in the HTS tapes/strands, and of an appropriate description of the voltage current (*V-I*) curve for the resistive transition of the SC materials. Note that the coupling to a (leastwise

simplified) electro-dynamic model for the cable is advisable at least for AC cables in normal operating conditions, in view of the presence of AC losses.

- Inclusion of parasitic heat from environment by radiation with an appropriate formulation, as that adopted already in the models based on the VE formulation (54). Note that radiation from the environment has never been considered relevant in LTS devices such those adopted for instance in the nuclear fusion field. For them, the contribution from the environment is typically neglected, mainly because the fusion cables are typically inserted into cryostats with a thermal shield at cryogenic temperature.

The inclusion also of a simplified model of the cryogenic system at the terminations of the cable, could help coping with transient situations where the inlet coolant conditions can deviate from the nominal values. In the case of the LTS cables for fusion, a lumped 0D modelling of the largest part of the auxiliaries has been proven to be adequate to provide reliable boundary conditions to the thermal-hydraulic simulations of the cables (72).

As far as the numerical aspects are concerned, the overall model should be able to cope with very long cable lengths, keeping the computational cost as low as possible. This need typically discourages the adoption of fully 3D models. The VEM, applied to 2D models, appear a robust and flexible method for this application. However, adaptive (as opposed to static) non-uniform spatial grids should be considered to capture steep-gradients region (such as local quench fronts) travelling along the cable, as an alternative to the switch to higher-order spatial discretization or to local high-order interpolation recipes. An adaptive time stepping should allow capturing the different time-scales involved in the cable operations in a computationally-effective way.

The robustness of the model with the peculiarities highlighted above should be proved through a clear and transparent Verification and Validation (V&V) process (73). An open-source tool, with open model and open data, would help with an effective validation of the implemented models (larger database availability), allowing at the same time a wide sharing of model improvements. Furthermore, an open-source tool would very well fit in the framework of the Open Science, promoted by the European Community (74), and already pioneered by some researchers (66) in this field.

5. Conclusions

The SCTCs and SCTLs can have different layouts and their operation is typically characterized by a very tight temperature (and pressure) range, especially if the cheaper LN_2 is adopted as cryogen. As today, a model able to reliably describe the cooling, i.e. the transient thermal-fluid behavior, of the SCTCs in normal and off normal conditions, capable of coping with different cable layouts and different cryogens, is not available to the best of our knowledge. The relevant ingredients of such model, reflecting the best peculiarities of already available models, have been identified and complemented with additional features that comes from the experience in the adjacent field of the LTS cable modelling. A model capable to take into account all the pointed features, once suitably verified and validated, should be able to support the design, tests and development of SCTCs, which are needed to bring this

technology to its technology maturity, contributing to the energy transition. In this framework, the openness of the numerical tools, models and data would be beneficial.

Acknowledgements

References

1. European Commission. The European Green Deal [Internet]. 2019. Available from: https://eur-lex.europa.eu/legal-content/EN/TXT/?qid=1576150542719&uri=COM%3A2019%3A640%3AFIN

2. Sytnikov VE, Bemert SE, Krivetsky I V., Karpov VN, Romashov MA, Shakarian YG, et al. The Test Results of AC and DC HTS Cables in Russia. IEEE Trans Appl Supercond. 2016 Apr 1;26(3).

3. Thomas H, Marian A, Chervyakov A, Stückrad S, Salmieri D, Rubbia C. Superconducting transmission lines - Sustainable electric energy transfer with higher public acceptance? Vol. 55, Renewable and Sustainable Energy Reviews. Elsevier Ltd; 2016. p. 59–72.

4. High Temperature Superconductor (HTS) Cables - ENTSO-E [Internet]. [cited 2021 May 10]. Available from: https://www.entsoe.eu/Technopedia/techsheets/high-temperature-superconductor-hts-cables

5. Doukas DI. Superconducting Transmission Systems: Review, Classification, and Technology Readiness Assessment. IEEE Trans Appl Supercond. 2019 Aug 1;29(5).

6. Lee C, Son H, Won Y, Kim Y, Ryu C, Park M, et al. Progress of the first commercial project of higherature superconducting cables by KEPCO in Korea. Supercond Sci Technol [Internet]. 2020 Feb 17 [cited 2021 May 11];33(4):044006. Available from: https://iopscience.iop.org/article/10.1088/1361-6668/ab6ec3

7. Bae Na J, Gyung Sung H, Yeol Choi C, Jang Y, Hun Y. Design of 23kV 50MVA class HTS Cable in South Korea. J Phys. 2018;12073.

8. Yamaguchi S, Ivanov Y, Watanabe H, Chikumoto N, Koshiduka H, Hayashi K, et al. Construction and 1st Experiment of the 500-meter and 1000-meter DC Superconducting Power Cable in Ishikari. In: Physics Procedia. Elsevier B.V.; 2016. p. 182–6.

9. Chikumoto N, Watanabe H, Ivanov Y V., Takano H, Yamaguchi S, Ishiyama K, et al. Second Cooling Test of 1000-m Superconducting DC Cable System in Ishikari. IEEE Trans Appl Supercond. 2018 Jun 1;28(4).

10. Sytnikov VE, Bemert SE, Ivanov Y V., Kopylov SI, Krivetskiy I V., Rimorov DS, et al. HTS DC Cable line project: On-Going activities in Russia. IEEE Trans Appl Supercond. 2013;23(3).

11. Sytnikov VE, Bemert SE, Kopylov SI, Romashov MA, Ryabin T V., Shakaryan YG, et al. Status of HTS cable link project for St. Petersburg Grid. IEEE Trans Appl Supercond. 2015 Jun 1;25(3).

12. Sytnikov V, Kashcheev A, Dubinin M, Karpov V, Ryabin T. Test Results of the Full-Scale HTS Transmission Cable Line (2.4 Km) for the St. Petersburg Project. IEEE Trans Appl Supercond. 2021;

13. Stemmle M, Merschel F, Noe M, Hobl A. Ampacity project - Worldwide first superconducting cable and fault current limiter installation in a German city center. In: IET Conference Publications. 2013.

14. Stemmle M, Merschel F, Noe M, Hobl A. AmpaCity - Advanced superconducting medium voltage system for urban area power supply. In: Proceedings of the IEEE Power Engineering Society Transmission and Distribution Conference. Institute of Electrical and Electronics Engineers Inc.; 2014.

15. Stemmle M, Allweins K, Merschel F, Kugel T, Herzog F, Kutz T, et al. Three years operation experience of the AmpaCity system installation in Essen, Germany. EUCAS. 2017.

16. Li J, Zhang L, Ye X, Xia F, Cao Y. Demonstration Project of 35 kV/1 kA Cold Dielectric High Temperature Superconducting Cable System in Tianjin. IEEE Trans Appl Supercond [Internet]. 2020 Mar;30(2):1–5. Available from: https://ieeexplore.ieee.org/document/8947956/

17. Xie W, Wei B, Yao Z. Introduction of 35 kV km Level Domestic Second Generation High Temperature Superconducting Power Cable Project in Shanghai, China [Internet]. Vol. 33, Journal of Superconductivity and Novel Magnetism. Springer; 2020 [cited 2021 May 11]. p. 1927–31. Available from: https://doi.org/10.1007/s10948-020-05508-z

18. Maguire JF, Schmidt F, Bratt S, Welsh TE, Yuan J, Allais A, et al. Development and demonstration of a HTS power cable to operate in the long island power authority transmission grid. In: IEEE Transactions on Applied Superconductivity. 2007. p. 2034–7.

19. Schmidt F, Maguire J, Welsh T, Bratt S. Operation experience and further development of a high- Temperature superconducting power cable in the long island power authority grid. In: Physics Procedia. Elsevier B.V.; 2012. p. 1137–44.

20. Kirby NM, Macleod NM, Stidham D, Reynolds M. Tres Amigas: A flexible gateway for renewable energy exchange between the three asynchronous AC networks in the USA. In: 44th International Conference on Large High Voltage Electric Systems 2012. 2012.

21. Cheetham P, Ravindra H, Stamm T, Park C, Kim C, Graber L, et al. High Temperature Superconducting Power Cables for MVDC Power Systems of Navy Ships. In: 2019 IEEE Electric Ship Technologies Symposium, ESTS 2019. Institute of Electrical and Electronics Engineers Inc.; 2019. p. 548–55.

22. Ferrara PJ, Uva MA, Nowlin J. Naval ship-to-shore high temperature superconducting power transmission cable feasibility. IEEE Trans Appl Supercond. 2011 Jun;21(3 PART 2):984–7.

23. Fetisov SS, Zubko V V., Zanegin SY, Nosov AA, Vysotsky VS, Kario A, et al. Development and characterization of a 2G HTS roebel cable for aircraft power systems. IEEE Trans Appl Supercond. 2016 Apr 1;26(3).

24. Suttell NG, Vargas JVC, Ordonez JC, Pamidi S V., Kim CH. Modeling and optimization of gaseous helium (GHe) cooled high temperature superconducting (HTS) DC cables for high power density transmission. Appl Therm Eng. 2018 Oct 1;143:922–34.

25. Zanino R, Richard LS. Multiscale approach and role of validation in the thermal-hydraulic modeling of the ITER superconducting magnets. IEEE Trans Appl Supercond. 2013;23(3).

26. Bruzek CE. Introduction to superconducting power cable systems [Internet]. 2016 [cited 2021 Jul 8]. p. 1–43. Available from: http://www.die.ing.unibo.it/pers/morandi/didattica/Tempora

ry-ESAS-summer-school-Bologna-2016/Bruzek.pdf

27. Kosaki M, Nagao M, Mizuno Y, Kyougoku M, Horii K, Shimizu N. Development of cross-linked polyethylene insulated superconducting cable. In: Proceedings of the Symposium on Electrical Insulating Materials. Publ by Inst of Electrical Engineers of Japan; 1988. p. 79–82.

28. Saugrain J-M, Schmidt F, Mirebeau P. SUPERCONDUCTING CABLES-STATUS AND APPLICATIONS. In: Jicable [Internet]. 2007 [cited 2021 Jul 8]. Available from: http://www.jicable.org/TOUT_JICABLE_FIRST_PAGE/20 07/2007-A3-1_page1.pdf

29. Bruzek CE, Ballarino A, Escamez G, Giannelli S, Grilli F, Lesur F, et al. Cable Conductor Design for the High-Power MgB2 DC Superconducting Cable Project of BEST PATHS. IEEE Trans Appl Supercond. 2017 Jun 1;27(4).

30. Stamm T, Cheetham P, Park C, Kim CH, Graber L, Pamidi S. Novel gases as electrical insulation and a new design for gas-cooled superconducting power cables. IEEE Electr Insul Mag. 2020 Sep 1;36(5):32–42.

31. Bottura L. Thermal, Hydraulic, and Electromagnetic Modeling of Superconducting Magnet Systems. IEEE Trans Appl Supercond. 2016 Apr 1;26(3).

32. Hu N, Toda M, Ozcivan AN, Yagai T, Tsuda M, Hamajima T. Fault current analysis in a tri-axial HTS cable. In: IEEE Transactions on Applied Superconductivity. 2010. p. 1288–91.

33. Fuchino S, Furuse M, Higuchi N. Longitudinal temperature distribution in superconducting power cables with counter-flow cooling. In: IEEE Transactions on Applied Superconductivity. 2002. p. 1339–42.

34. Ha SK, Kim SK, Kim JG, Park M, Yu IK, Lee S, et al. Transient characteristic analysis of a tri-axial HTS power cable using PSCAD/EMTDC. IEEE Trans Appl Supercond. 2013;23(3).

35. Angeli G, Bocchi M, Ascade M, Rossi V, Valzasina A, Martini L. Development of Superconducting Devices for Power Grids in Italy: Update about the SFCL Project and Launching of the Research Activity on HTS Cables. IEEE Trans Appl Supercond. 2017 Jun 1;27(4).

36. Leachman JW, Jacobsen RT, Lemmon EW, Penoncello SG. Thermodynamic Properties of Cryogenic Fluids [Internet]. Cham: Springer International Publishing; 2017 [cited 2021 May 20]. (International Cryogenics Monograph Series). Available from: http://link.springer.com/10.1007/978-3-319-57835-4

37. Katheder H. Optimum thermohydraulic operation regime for cable in conduit superconductors (CICS). Cryogenics (Guildf). 1994 Jan 1;34(SUPPL. 1):595–8.

38. Furuse M, Fuchino S, Agatsuma K, Masuda T, Ohya M, Honjo S, et al. Stability analysis of HTS power cable with fault currents. IEEE Trans Appl Supercond. 2011 Jun;21(3 PART 2):1021–4.

39. GASPAK [Internet]. [cited 2021 Jul 8]. Available from: https://htess.com/gaspak/

40. Sato Y, Agatsuma K, Wang X, Ishiyama A. Temperature and pressure simulation of a high-temperature superconducting cable cooled by subcooled LN2 with fault current. IEEE Trans Appl Supercond. 2015 Jun 1;25(3).

41. Yumura H, Ashibe Y, Ohya M, Itoh H, Watanabe M, Masuda T, et al. Update of YOKOHAMA HTS cable project. IEEE Trans Appl Supercond. 2013;23(3).

42. Yasui T, Takeda N, Yokoo Y, Agatsuma K, Ishiyama A, Wang X, et al. Temperature and Pressure Distribution Simulations of 3-km-Long High-Temperature Superconducting Power Cable System with Fault Current for 66-kV-Class

Transmission Lines. IEEE Trans Appl Supercond. 2017 Jun 1;27(4).

43. Maruyama O, Ohkuma T, Izumi T, Shiohara Y. Numerical Analysis of Heat Transfer and Fluid Characteristics of Flowing Liquid Nitrogen in HTS Cable. In: Physics Procedia. Elsevier B.V.; 2014. p. 330–3.

44. Zhou Z, Zhu J, Li H, Qiu M, Li Z, Ding K, et al. Magnetic-thermal coupling analysis of the cold dielectric high temperature superconducting cable. IEEE Trans Appl Supercond. 2013;23(3).

45. Ciotti M, Nijhuis A, Ribani PL, Richard LS, Zanino R. THELMA code electromagnetic model of ITER superconducting cables and application to the ENEA stability experiment. Supercond Sci Technol [Internet]. 2006 Oct 1 [cited 2021 May 29];19(10):987–97. Available from: https://iopscience.iop.org/article/10.1088/0953-2048/19/10/001

46. Del-Rosario-Calaf G, Lloberas-Valls J, Sumper A, Granados X, Villafafila-Robles R. Modeling of second generation HTS cables for grid fault analysis applied to power system simulation. IEEE Trans Appl Supercond. 2013;23(3).

47. De Sousa WTB, Kottonau D, Bock J, Noe M. Investigation of a Concentric Three-Phase HTS Cable Connected to an SFCL Device. IEEE Trans Appl Supercond. 2018 Jun 1;28(4).

48. Kottonau D, De Sousa WTB, Bock J, Noe M. Design Comparisons of Concentric Three-Phase HTS Cables. IEEE Trans Appl Supercond. 2019 Sep 1;29(6).

49. Shabagin E, Heidt C, Strauß S, Grohmann S. Modelling of 3D temperature profiles and pressure drop in concentric three-phase HTS power cables. Cryogenics (Guildf). 2017 Jan 1;81:24–32.

50. Hu N, Toda M, Watanabe T, Tsuda M, Hamajima T. Recovery time analysis in a tri-axial HTS cable after an over-current fault. In: Physica C: Superconductivity and its Applications. North-Holland; 2011. p. 1295–9.

51. Choi Y, Kim D, Lee C, Won D, Yoo J, Yang H, et al. Thermo-hydraulic analysis of a tri-axial high-temperature superconducting power cable with respect to installation site geography. Energies [Internet]. 2020 Aug 1 [cited 2021 Jul 1];13(15):3898. Available from: www.mdpi.com/journal/energies

52. Heat Transfer and Fluid Flow Analysis Software, SINDA/FLUINT [Internet]. [cited 2021 Jul 9]. Available from: https://www.crtech.com/products/sindafluint

53. Yang S, Ordonez JC. Development of Generic Superconducting Components Library in MATLAB/Simulink for Thermal-Hydraulic Analyses. IEEE Trans Appl Supercond. 2021;31(5):0600405.

54. Souza JA, Ordonez JC, Hovsapian R, Vargas JVC. Thermal modeling of helium cooled high-temperature superconducting DC transmission cable. IEEE Trans Appl Supercond. 2011 Jun;21(3 PART 2):947–52.

55. Suttell NG, Vargas JVC, Ordonez JC. Transient Thermal Analysis of HTS DC Cables Cooled with Gaseous Helium Using a Volume Element Method Transactions on Applied Superconductivity. IEEE Trans Appl Supercond. 2017 Jun 1;27(4).

56. Buiar, Celso L.;Vargas JVC. Thermodynamic analysis applied to superconducting DC cable model. In: Proceedings of the 14th Brazilian Congress of Thermal SCiences and Engineering. 2012.

57. Ordonez JC, Souza JA, Shah DR, Vargas JVC, Hovsapian R. Temperature and Pressure Drop Model for Gaseous Helium Cooled Superconducting DC Cables. IEEE Trans Appl

Supercond. 2013 Jan 21;23(3):5402005–5402005.

58. Buiar, Celso L.; Vargas, José V. C.; Ordonez JC. Dimensionless high tempeature superconducting (HTS) DC cable model. In: Proceedings of the 22nd International Congress of Mechanical Engineering. 2013.

59. Kim CH, Kim SK, Graber L, Pamidi S V. Cryogenic thermal studies on terminations for helium gas cooled superconducting cables. In: Physics Procedia. Elsevier B.V.; 2015. p. 201–7.

60. Suttell N, Kim CH, Ordonez J, Shah D, Graber L, Pamidi S. Thermal modeling of gaseous helium as a cryogen for high temperature superconducting cable components. IEEE Trans Appl Supercond. 2015 Jun 1;25(3).

61. Doukas DI, Chrysochos AI, Papadopoulos TA, Labridis DP, Harnefors L, Velotto G. Volume Element Method for Thermal Analysis of Superconducting DC Transmission Cable. IEEE Trans Appl Supercond. 2017 Jun 1;27(4).

62. Corsaro P, Bechis M, Caracino P, Castiglioni W, Cavalleri G, Coletta G, et al. Manufacturing and commissioning of 24 kV superconducting cable in Detroit. Phys C Supercond its Appl. 2002 Oct 1;378–381(PART 2):1168–73.

63. Doukas DI, Chrysochos AI, Papadopoulos TA, Labridis DP, Harnefors L, Velotto G. Coupled Electro-Thermal Transient Analysis of Superconducting DC Transmission Systems Using FDTD and VEM Modeling. IEEE Trans Appl Supercond. 2017 Dec 1;27(8).

64. Suttell NG, Kim CH, Pamidi S V., Ordonez JC. Transient Cryogenic Thermal Modeling of HTS Cable Systems Cooled with Gaseous Helium Transactions on Applied Superconductivity. IEEE Trans Appl Supercond. 2017 Jun 1;27(4).

65. De Sousa WTB, Kottonau D, Noe M. Transient Simulation and Recovery Time of a Three-Phase Concentric HTS Cable. IEEE Trans Appl Supercond. 2019 Aug 1;29(5).

66. De Sousa WTB, Shabagin E, Kottonau D, Noe M. An open-source 2D finite difference based transient electro-thermal simulation model for three-phase concentric superconducting power cables. Supercond Sci Technol. 2020 Dec 7;34(1):015014.

67. Lee S-J, Sung H-J, Park M, Won D, Yoo J, Yang HS. Analysis of the Temperature Characteristics of Three-Phase Coaxial Superconducting Power Cable according to a Liquid Nitrogen Circulation Method for Real-Grid Application in Korea. Energies [Internet]. 2019 May 8 [cited 2021 May 10];12(9):1740. Available from: https://www.mdpi.com/1996-1073/12/9/1740

68. He J, Tang Y, Wei B, Li J, Ren L, Shi J, et al. Thermal analysis of HTS power cable using 3-D FEM model. IEEE Trans Appl Supercond. 2013;23(3).

69. Maruyama O, Ohkuma T, Izumi T, Shiohara Y. Numerical calculation of advection heat transfer and fluid flow dynamics of LN2 flowing HTS cable. IEEE Trans Appl Supercond. 2015 Jun 1;25(3).

70. Savoldi L, Zanino R. M & M: Multi-conductor Mithrandir code for the simulation of thermal-hydraulic transients in superconducting magnets. Cryogenics (Guildf). 2000;

71. Savoldi Richard L, Casella F, Fiori B, Zanino R. The 4C code for the cryogenic circuit conductor and coil modeling in ITER. Cryogenics (Guildf). 2010;

72. Zanino R, Bonifetto R, Casella F, Savoldi Richard L. Validation of the 4C code against data from the HELIOS loop at CEA Grenoble. In: Cryogenics. Elsevier; 2013. p. 25–30.

73. Oberkampf WL, Roy CJ. Verification and validation in scientific computing [Internet]. Verification and Validation in Scientific Computing. Cambridge University Press; 2011 [cited 2021 Jul 9]. 1–767 p. Available from: https://www.cambridge.org/core/books/verification-and-validation-in-scientific-computing/05CA1F8F3CCB5AE5445FDF55239A0183

74. Open Science European Commission [Internet]. [cited 2021 Jul 9]. Available from: https://ec.europa.eu/info/research-and-innovation/strategy/strategy-2020-2024/our-digital-future/open-science_en